

# Tracking Triggers for the HL-LHC

Anders Ryd<sup>1</sup> and Louise Skinnari<sup>2</sup>

<sup>1</sup>Department of Physics, Cornell University, Ithaca, NY 14853, USA;  
email: Anders.Ryd@cornell.edu

<sup>2</sup>Department of Physics, Northeastern University, Boston, MA 02115, USA;  
email: l.skinnari@northeastern.edu

Annu. Rev. Nucl. Part. Sci. 2020. 70:1–26

<https://doi.org/10.1146/annurev-nucl-020420-093547>

Copyright © 2020 by Annual Reviews.  
All rights reserved

## Keywords

charged particle tracking, trigger, CMS, ATLAS, HL-LHC

## Abstract

Hardware-based track reconstruction in the CMS and ATLAS trigger systems for the High-Luminosity LHC upgrade will provide unique capabilities. An overview is presented of earlier track trigger systems at hadron colliders, in particular for the Tevatron CDF and DØ experiments. We discuss the plans of the CMS and ATLAS experiments to implement hardware-based track reconstruction for the High-Luminosity LHC. Particular focus is placed on the track trigger capability of the upgraded CMS experiment. We discuss the challenges and opportunities of this novel handle, and review the alternatives that were considered for its implementation as well as discuss the expected performance. The planned track trigger systems for CMS and ATLAS have different goals, and we compare and contrast the two approaches.

## Contents

1. INTRODUCTION .....	2
1.1. Challenges and Requirements at the HL-LHC .....	3
1.2. Motivation for Hardware-Based Tracking .....	3
1.3. Early Developments .....	4
2. CMS TRACK TRIGGER .....	6
2.1. Outer Tracker for HL-LHC .....	7
2.2. Trigger Architecture .....	11
2.3. L1 Track Reconstruction Approaches .....	11
2.4. HL-LHC Track-Finding System .....	19
3. ATLAS HARDWARE-BASED TRACKING FOR HL-LHC .....	21
4. SUMMARY .....	24

## 1. INTRODUCTION

A critical component of any high-energy particle physics collider experiment is deciding which collision events to read out and save for future analysis, and which ones to discard. At the Large Hadron Collider (LHC) (1, 2) at CERN, proton-proton ( $pp$ ) collisions occur every 25 ns, corresponding to a beam crossing frequency of 40 MHz. For the ATLAS (3) and CMS (4) experiments, a typical collision event had a size of  $\sim 1$  MB during LHC Run 1–3. This corresponds to a data rate of roughly 40 TB per second, a rate much too large to both read out from the detectors and to store offline. Instead, only a small fraction of  $pp$  collisions is kept, made possible by the comparatively low cross sections for the physics processes of interest compared to the total LHC cross section. The system utilized to decide which collision events to retain is referred to as the *trigger system*. It typically consists of an initial hardware-based level implemented in custom electronics boards, as well as a high-level trigger implemented in software.

The High-Luminosity LHC (HL-LHC) upgrade (5, 6), planned for installation in 2025–2027, will significantly increase the instantaneous luminosity. As a consequence, a large increase in the number of simultaneous  $pp$  interactions within the same bunch crossing, known as *pileup*, is also expected. This is a challenge particularly for the hardware-based trigger; novel handles are required for ATLAS and CMS to mitigate these effects.

The identification of charged-particle trajectories (tracking) using silicon-based detectors is central to the LHC experiments. However, thus far, this has been restricted to software-based algorithms implemented in commercial CPUs in the high-level trigger or in the offline event reconstruction. In this review, we discuss the developments of hardware-based tracking (track triggering), specifically utilizing inputs from silicon tracking detectors. The focus of the review is the development that is underway for the CMS experiment for the HL-LHC operation to incorporate full-detector track reconstruction in the initial trigger level at an input rate of 40 MHz. We discuss the motivation and physics potential for utilizing hardware-based tracking, the associated challenges at the HL-LHC, and review prior developments in this area. Details are provided about the CMS track trigger system, including the design of the new outer tracker for HL-LHC, as well as the different track finding approaches that have been studied, along with their implementation. We discuss the foreseen HL-LHC track-finding system that will be based on field-programmable gate

arrays (FPGAs), the hardware platforms to be used, as well as the expected performance. The plans for the ATLAS experiment to incorporate hardware-based tracking for HL-LHC are also reviewed. We discuss the foreseen new tracking detector, two alternative trigger architectures, and the approach identified for performing the track reconstruction. Finally, a summary and conclusion is given.

### 1.1. Challenges and Requirements at the HL-LHC

The HL-LHC era offers exciting physics possibilities albeit with a substantially increased instantaneous luminosity, which is experimentally challenging. The detector systems will therefore undergo significant upgrades in order to maximally take advantage of the physics potential of the HL-LHC data sets. The main challenge of the HL-LHC operation for the ATLAS and CMS experiments is the large increase in the number of simultaneous  $pp$  interactions. At the LHC design luminosity, an average of 25  $pp$  interactions occur in each bunch crossing, whereas at the HL-LHC, an average of 200 simultaneous interactions are expected.

The large increase in pileup results in many more particles produced in each bunch collision, and consequently, an ambient increased energy in the calorimeter measurements, an increased number of low-momentum muons that could be misidentified as high-momentum ones, and so forth. Improving the experimental handles to identify particles in the trigger is thus required. A second experimental challenge of the HL-LHC operation is high radiation levels that, in particular, the innermost detector systems must accommodate. Radiation tolerance is thus a key requirement in the design of the silicon tracker. Consequently, the ATLAS and CMS experiments will improve the trigger systems, entirely replace the inner silicon-based tracking detectors, and upgrade large components of the readout systems associated with the muon and calorimeter systems.

### 1.2. Motivation for Hardware-Based Tracking

The motivation for identifying charged-particle trajectories in a hardware-based trigger system is two-fold. First, it is a powerful handle to improve the identification of different types of particles and, consequently, to enable the physics goals of the experiments. Second, the inclusion of charged particle trajectories is a novel experimental handle in the trigger that can facilitate entirely new analyses in currently unexplored corners of phase space.

The HL-LHC accelerator upgrade will increase the instantaneous luminosity for  $pp$  collisions to roughly  $7.5 \times 10^{34} \text{ cm}^{-2}\text{s}^{-1}$ , about four times larger than the maximum instantaneous luminosity at the LHC. The target during the HL-LHC operation is to collect data sets of  $3,000 \text{ fb}^{-1}$  for each of the ATLAS and CMS experiments, an order of magnitude larger than the full LHC data sets. The large data samples will enable detailed studies of rare Standard Model (SM) processes, precise Higgs boson ( $H$ ) measurements, and extend sensitivity in searches for particles and interactions beyond the SM (7, 8, 9, 10, 11). Extensive studies of the  $H$  boson production modes, properties, and interactions is a key goal. Rare decays, e.g. to  $\mu^+\mu^-$  and  $Z\gamma$ , are expected to be conclusively observed. The  $H$  boson self-coupling, which probes the Higgs field potential, will be studied through measuring the extremely rare  $HH$  production process. Other important tests of electroweak symmetry breaking include measurements of electroweak multiboson interactions and studies of quartic boson couplings, all low cross section processes that are currently not well constrained. In the flavor sector, the increased integrated luminosity will particularly benefit measure-

ments of rare  $b$  and  $c$  hadron decays, an indirect probe of beyond-SM physics, and can significantly improve searches for e.g. top quark flavor-changing neutral currents. Direct new physics searches, e.g. for signatures of supersymmetry, dark matter candidates, or new heavy gauge bosons, will be probed to higher mass scales.

The above studies rely on the capability of the experiments to identify, at the trigger level, physics objects at the electroweak scale with high efficiency. Momentum thresholds must be maintained sufficiently low to capture leptons and hadronic  $\tau$  decays from  $W/Z/H$  boson decays and low transverse momentum ( $p_T$ ) jets associated with  $b$  quarks. The searches for new physics, e.g. supersymmetry, require the identification of multiple low- $p_T$  objects, searches for dark matter particles typically relies on the triggering capability of missing transverse momentum, and so forth.

The ATLAS and CMS trigger systems for LHC Run 1–3 read out merely about 0.25% of the LHC collisions, or 100 kHz, from the initial hardware-based (Level-1, or L1) trigger. Following the software-based trigger, this data rate is reduced even further to about 1 kHz (12, 13). These L1 trigger systems utilize only information from the calorimeter and muon systems. To maintain the triggering capability at the HL-LHC while keeping the trigger rate at a manageable level, the trigger systems must be upgraded and improved. The inclusion of charged-particle tracking is a critical component in this. The precise measurement of a trajectory’s transverse momentum improves the identification of muons, reducing the rate of low- $p_T$  muons that are misidentified as a high- $p_T$  ones; an example of this is illustrated for the CMS experiment in Fig. 1. Track information also improves electron identification by matching tracks to calorimeter clusters, the reconstruction of hadronic  $\tau$  decays, and allows a selection based on tracks of charged ( $e, \mu, \tau$ ) and neutral ( $\gamma$ ) particles that are isolated from other activity in the detector to reduce event rates. Beyond improving the identification of individual trigger objects, tracking can be used in defining event-level quantities, e.g. the primary collision vertex to measure global quantities (e.g. the missing transverse momentum), and in correlating multiple objects when defining trigger signatures.

The inclusion of track reconstruction in the hardware-based trigger can also enable entirely new studies, probing physics processes that could previously not be identified in the trigger, e.g. due to overwhelming background processes when relying only on information from the calorimeter and muon system. Such signatures include e.g. displaced trajectories from hypothetical exotic long-lived particles and  $B$  physics processes with low- $p_T$  final-state particles (15). The full physics capability of incorporating tracking in the L1 trigger is yet to be explored.

The LHCb experiment, specialized for studying charm and beauty physics, is being upgraded during the LHC Long Shutdown 2 in 2019–2021 (16). Since the fraction of  $pp$  collisions containing charm or beauty quarks is very high, and the instantaneous luminosity for LHCb is lower than for ATLAS and CMS, these upgrades use a different strategy for selecting the interesting collisions. LHCb is implementing a trigger-less system where all collisions at an input rate of about 30 MHz are read out from the detector, and the events are processed in the event filter farm, which is a fully software-based trigger.

### 1.3. Early Developments

Track triggers for various applications have been used at many particle physics experiments. Some examples include track identification in  $e^+e^-$  experiments, e.g. BABAR and Belle (17, 18), and identification of long-lived particles, e.g. at HERA-B (19). The early applications

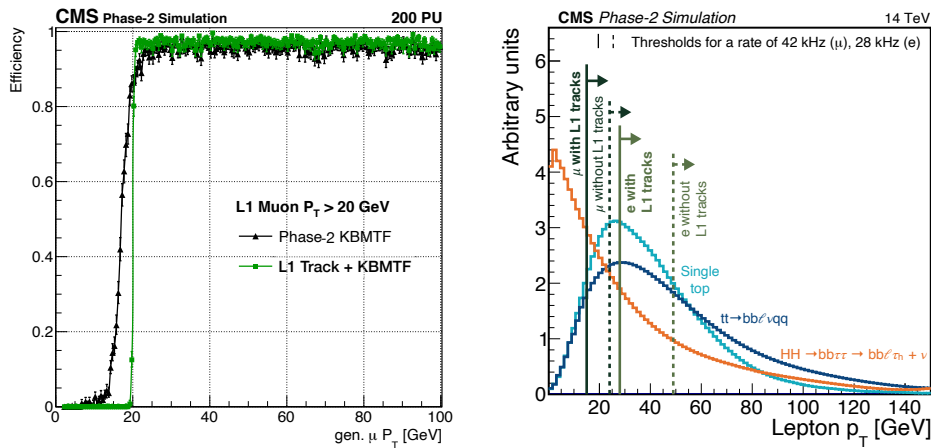


**Figure 1**

Example of the power of including L1 tracking in CMS for the HL-LHC. The left figure illustrates the improved muon momentum resolution when including tracks (Track + KBMTF) for the barrel muon track finder (Phase-2 KBMTF). The right figure shows simulated electron and muon  $p_T$  distributions from  $HH$ , single top quark, and semileptonic  $t\bar{t}$  decays. The solid (dashed) vertical lines correspond to the trigger thresholds with (without) using L1 tracks for a given trigger rate, assuming 200 pileup interactions. The addition of tracking information reduces the trigger rate through the resulting improved object identification. From Ref. (14).

of track triggers that most closely relates to the challenges at the HL-LHC were used to perform track and vertex identification at the CDF and  $D\phi$  (20, 21) hadron collider experiments at the Tevatron proton-antiproton ( $p\bar{p}$ ) collider at Fermilab. Developments for the ATLAS Fast TracKer (FTK) system (22) also provides important guidance toward the upgrades for the HL-LHC. Here, a brief review of the earlier track trigger developments at hadron colliders is provided.

The CDF and  $D\phi$  experiments were upgraded for Run 2 of the Tevatron to provide additional experimental capabilities. In particular, this included new or expanded capabilities for tracking and track triggering. Both experiments provided tracking in their outer tracking detectors at the full bunch collision rate to provide improved triggering of muons and other particles. In addition, tracks in the outer trackers were combined with more precise hits from the silicon tracking detectors to provide precise impact parameter measurements for the identification of long-lived particles from e.g.  $b$  hadrons. The CDF and  $D\phi$  track triggers operated in an environment with bunch crossings every 396 ns (2.5 MHz) and an average pileup of about 4 to 5. In comparison, at the HL-LHC bunch collisions will take place every 25 ns (40 MHz) with an average pileup of about 200.

The CDF II Silicon Vertex Tracker (SVT) (20) made use of measurements from the Silicon Vertex Tracker (SVXII) and the Central Outer Tracker (COT) to reconstruct precise 2-D trajectories of charged particles. The CDF track trigger used two stages, the first was the eXtremely Fast Tracker (XFT) (23, 24) that used hits from the COT to reconstruct charged particle trajectories. The XFT first found track segments in four adjacent cells consistent with  $p_T > 1.5$  GeV. The segments were linked together to form complete tracks. The SVT in the second stage was implemented using Associative Memories (AM) (25) where

the input was hits from the SVXII detector and the XFT tracks. The AM-based pattern recognition was implemented using 64 sectors in  $\phi$ . Each sector used two AM boards that had 128 AM chips, each with 128 patterns for a total of 32k patterns for a sector. The patterns found in the AM were forwarded to the track fitting stage, implemented in FPGAs. The track fit was performed using a linearized  $\chi^2$  fit.

The DØ experiment implemented track reconstruction in their L1 Central Track Trigger (L1CTT) (21) using hits from the Central Fiber Tracker (CFT) (26). The track finding was implemented using FPGAs in  $4.5^\circ$  sectors. Each sector used four FPGAs for track finding in different  $p_T$  ranges ( $> 10$  GeV, 5 to 10 GeV, 3 to 5 GeV, and 1.5 to 3 GeV). A track was required to have hits in all eight axial CFT layers. The pattern recognition was implemented using combinatorial logic in the FPGA. The number of track equations implemented in each FPGA varied from 3,000 for the highest  $p_T$  range to 10,000 for the lowest  $p_T$  range. The tracks found in groups of ten track finding sectors were collected in an octant board, which in turn found the sectors with the highest occupancy and identified isolated tracks that were used for the L1 trigger decision with a latency of  $2.5 \mu\text{s}$  with respect to the beam collision time. The L1 tracks were also used as input to the L2 track finding. The maximum input rate for the L2 trigger was 10 kHz. The L2 processor boards were based on 1 GHz Pentium processors. The Level-2 Silicon Tracking Trigger (L2STT) used tracks found in the L1CTT and added precise Silicon Microstrip Tracker hits. This allowed rejecting misreconstructed ("fake") L1CTT tracks, improving the  $p_T$  resolution, and most importantly it allowed identifying tracks from long-lived particles, in particular  $b$  hadrons (27), using the precise transverse impact parameter.

The ATLAS Collaboration developed a track trigger, FTK, for the Phase-1 upgrades. The FTK upgrade implemented global track reconstruction for events selected by the L1 trigger at a maximum rate of 100 kHz. The design goal of the FTK was to reconstruct tracks with  $p_T$  greater than 1 GeV. The FTK used hits from the semiconductor tracker (SCT), the pixel detector, and the insertable B-layer (IBL). The hits were organized into 12 logical detector layers, eight in the SCT and four in the pixel+IBL. The FTK was implemented using AMs for the pattern recognition, using 8 of the 12 layers. In a second stage, the hits found in the pattern recognition step were used for the final track fit, including also hits matched to the track in the four layers not used in the pattern recognition. The full ATLAS FTK system was not installed, but a slice of the system was operated during the Run 2 of the LHC (28).

## 2. CMS TRACK TRIGGER

A key goal of the CMS detector upgrades for the HL-LHC operation is to implement track finding at the L1 trigger level to keep thresholds sufficiently low to maintain high efficiency for electroweak physics. The goal of the CMS track trigger is to reconstruct trajectories of charged particles with  $p_T > 2$  GeV for all  $pp$  interactions. These tracks will be available in the L1 trigger and will provide much improved identification of objects such as muons, electrons, taus, and hadronic jets. To accomplish this goal, CMS has designed a silicon-based outer tracker (15) that is uniquely capable of producing trigger primitives, *stubs*, that are used to reconstruct the L1 tracks at 40 MHz.

## 2.1. Outer Tracker for HL-LHC

The CMS tracking detector will be replaced for the HL-LHC operation as the original detector would not be able to handle the expected data rate or radiation dose. The complete replacement of the tracking detector provides a unique opportunity to introduce new designs and capabilities. CMS has used this opportunity to design a tracker capable of providing  $p_T$  discrimination at the detector module level before readout. The CMS tracker for HL-LHC consists of an inner tracker (IT) with pixel sensors, which is not utilized in the L1 trigger, and an outer tracker (OT) with dedicated  $p_T$  modules. The ability to provide  $p_T$  discrimination results in a sufficient reduction of the data rate to allow readout of hits above a threshold of about 2 GeV for use in the L1 trigger. This unique detector design is essential in enabling full-detector track reconstruction at the full 40 MHz bunch crossing rate.

A charged particle produced at the interaction point follows a trajectory in the transverse plane in a uniform magnetic field along the beam-axis given by

$$\phi = \phi_0 + \arcsin\left(\frac{qB}{2p_T} \cdot r\right) \quad 1.$$

where  $\phi$  is the azimuthal position of the trajectory at radius  $r$ ,  $\phi_0$  is the particle azimuthal direction at the origin,  $B$  is the magnetic field strength,  $q$  is the particle charge, and  $p_T$  is the transverse momentum. For two hits with a radial separation of  $\Delta r$ , this corresponds to a  $\phi$  separation

$$\Delta\phi = \Delta r \frac{qB}{2p_T} \quad 2.$$

where the approximation  $\arcsin x = x$  has been used. The separation along the azimuthal direction  $x$  is given by

$$\Delta x = r \Delta r \frac{qB}{2p_T}. \quad 3.$$

The separation of hits is proportional to  $r$ ,  $\Delta r$ ,  $B$ , and inversely proportional to  $p_T$ .

The outer tracker design uses detector modules that consist of two silicon sensors separated by a few millimeters. By correlating hits between the two sensors, and making use of the bending in the CMS 3.8 T magnetic field, pairs of hits, referred to as stubs, with a small bend (high  $p_T$ ) can be selected. As illustrated in Fig. 2, this concept works both for barrel modules and modules in an endcap geometry. As the hit separation in the azimuthal direction is a function of the radial separation of the hits, the endcap geometry will require a larger sensor separation at large pseudorapidity ( $\eta$ ). The goal of the  $p_T$  modules is not to provide a precise momentum measurement, but to distinguish stubs with a transverse momentum greater than 2 GeV, a threshold that corresponds to a data volume reduction of  $\mathcal{O}(10)$ , so that these can be propagated to the back-end track finding system. The most challenging stub forming configuration is for the innermost barrel layer. At a radius of about 250 mm, a 2 GeV track will have a separation  $\Delta x$  of about 185  $\mu\text{m}$  for a sensor separation  $\Delta r$  of 2.6 mm. With a pitch between the silicon strips of about 100  $\mu\text{m}$ ,  $p_T$  discrimination can be implemented to reject stubs from low- $p_T$  trajectories. Though a larger sensor separation would increase the hit separation in the two sensors and provide a more precise  $p_T$  determination, the larger stub formation windows would increase the rate of combinatorial stubs. This is an issue in the inner region of the detector where the occupancy is high. In the outer part of the detector larger windows can be used since the probability of forming stubs from uncorrelated hits is smaller.

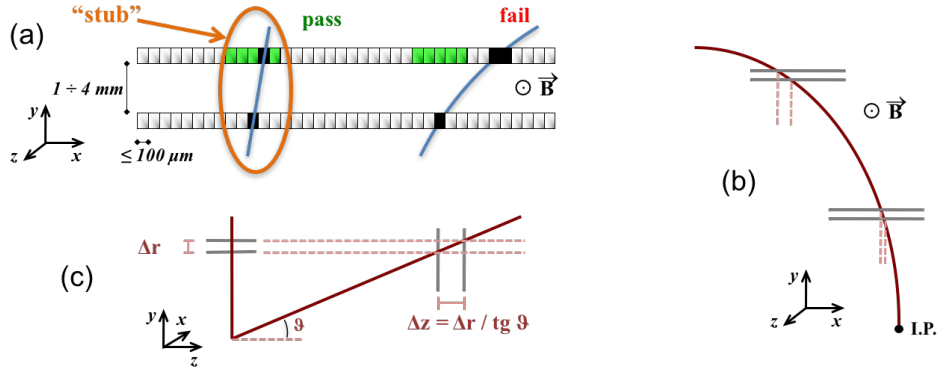


**Figure 2**

The principle for  $p_T$  discrimination in the outer tracker modules. (a) Correlation of signals in closely-spaced sensors enables the rejection of low- $p_T$  particles; the channels in green show the acceptance window to form a stub from the hit indicated in the inner sensor. (b) The same transverse momentum corresponds to a larger distance between the two hits at larger radii for a given sensor spacing. (c) For the endcap discs, a larger spacing between the sensors is needed to achieve the same discriminating power as in the barrel at the same radius. Figure adapted from Ref. (15).

The CMS tracker will make use of two types of  $p_T$  modules. The first type is the pixel-strip (PS) module in which one sensor tier consists of macro-pixels (1.446 mm long by  $100 \mu\text{m}$ ) and the other tier of strips (2.4 cm long). The other module type is the strip-strip (2S) module where both sensor tiers are strips (5 cm long and  $90 \mu\text{m}$  pitch). These modules are illustrated in Fig. 3. For both PS and 2S modules, hits are read out at the edges of the module and the data are communicated between the two sensor tiers through a flex circuit in order to correlate hits and produce stubs.

Stubs are formed in the MacroPixel ASIC (MPA) (29) in the PS modules and in the CMS Binary Chip (CBC) (30) in the 2S modules. The stubs formed in the front-end ASICs are communicated to the concentrator chips (CIC) (31). There are two CICs on each module; one for each readout side. The CICs implement load balancing by grouping stubs from eight consecutive bunch crossings before sending the payload to the back-end electronics via optical links. The CIC chips implement stub  $p_T$  ordering and discard the stubs with lowest  $p_T$  in case truncation is needed. Readout data and module configuration data are transmitted and received using one Low-power Gigabit Transceiver (LpGBT) (32) per module. Depending on the location in the detector (and thus the occupancy) the optical links are operated at either 5 or 10 Gbits/s.

The PS modules are used in the inner barrel layers and the inner half of the disks as they provide 3-D space points that allow precise  $z$  position measurements for the reconstructed tracks. The PS modules are also capable of handling the higher hit rate due to the finer segmentation with the macro-pixels and a smaller detector area.

The detector layout is shown for one quadrant of the detector in Fig. 4. There are six barrel layers with the inner three layers composed of PS modules (TBPS) and the outer three layers composed of 2S modules (TB2S). The modules in the forward region of the three inner layers are tilted such that charged particles from the interaction point (IP) will



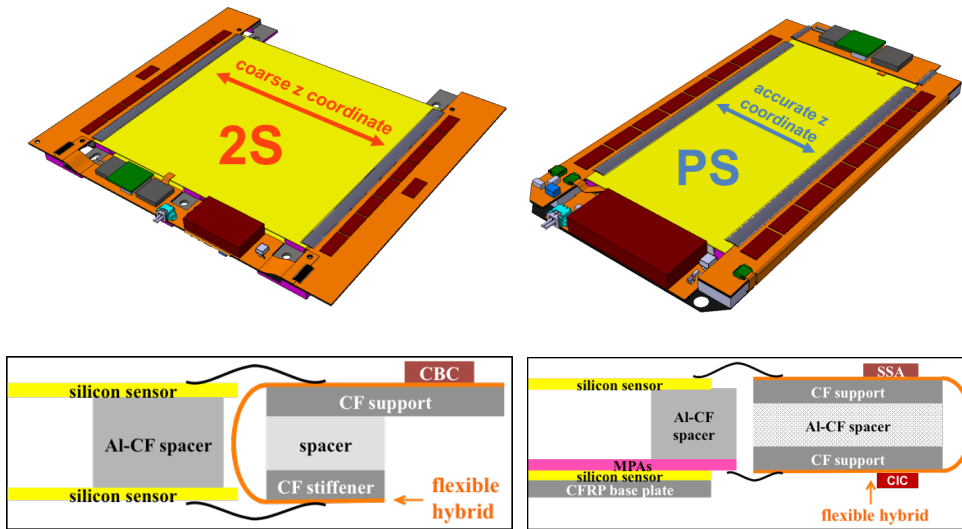


**Figure 3**

Illustration of the concept of the  $p_T$  modules for the upgraded CMS outer tracker for HL-LHC. The two types of modules, 2S and PS, are shown to the left and right, respectively. The top images show a layout of the two module types and the bottom images show a cross-sectional view of the connectivity at the edges of the modules. These figures illustrate how hit information is communicated between the two sensor tiers and correlations, stubs, are formed. In the 2S modules one CBC reads out the hits from both sensors and forms the correlations. For the PS modules, the strip sensor, at top in the figure, is read out by the SSA and the hits are communicated through the flexible hybrid to the MPA, which reads out the macro pixels and form the stubs. The separation between the sensors varies from 1.6 mm to 4.0 mm. From Ref. (15).

traverse the modules in a direction approximately perpendicular to the sensor plane. This increases the efficiency for reconstructing a stub since the particles are more likely to hit both sensors. It also reduces the sensor area needed to provide complete coverage. The PS modules in the TBPS use sensor spacings of 1.6 mm, 2.6 mm, or 4.0 mm depending on the position and orientation of the sensors, as shown in Fig. 4. The 2S modules in the barrel all have 1.8 mm spacing.

There are five disks (TEDD) on each side of the interaction point. Each disk has five outer rings of 2S modules with sensor spacings of 1.8 mm or 4.0 mm. The two disks closest to the IP extend somewhat closer to the beamline and have ten rings of PS modules while the outer three disks have seven rings of PS modules. Also shown in Fig. 4 is the stub acceptance window, in number of strips, for which hits in the two sensors are accepted as a stub. This window varies from as little as two strips in the PS modules at the lowest radii in the forward region to nine strips. For the 2S modules the acceptance window varies between 6–15 strips. These acceptance windows are configurable and can be tuned to manage the rate for the trigger data.

The simulated stub reconstruction efficiency as a function of particle  $p_T$  is shown in Fig. 5 for modules in the barrel and endcap regions. The stub finding windows are chosen to provide high efficiency at the 2 GeV threshold for track finding. In the innermost layer,

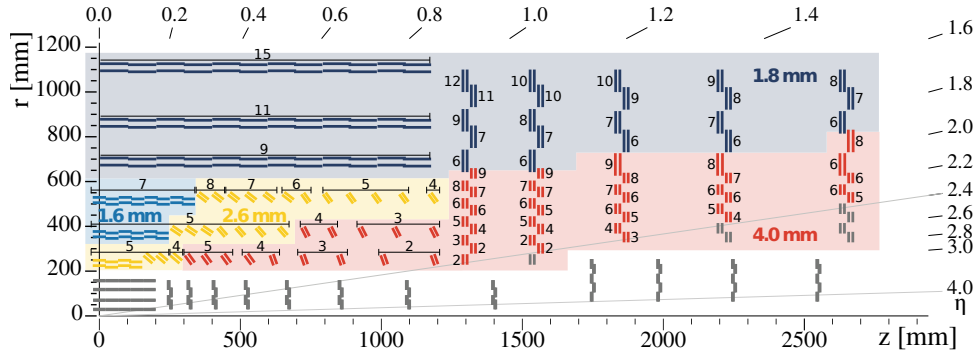


Figure 4

One quarter of the layout of the CMS outer tracker for HL-LHC, showing also the different module spacings and stub acceptance windows used. The PS modules are indicated in light blue, yellow, and red (the PS modules in grey are not used in the trigger). The different colors correspond to the sensor separation in the modules; blue is 1.6 mm, yellow is 2.6 mm, and red is 4.0 mm. The 2S modules are in dark blue or red and have 1.8 mm or 4.0 mm sensor spacing, respectively. The numbers in black next to the modules are the stub acceptance windows in number of strips. The inner pixel detector modules (grey) are not used in the L1 readout. From Ref. (15).

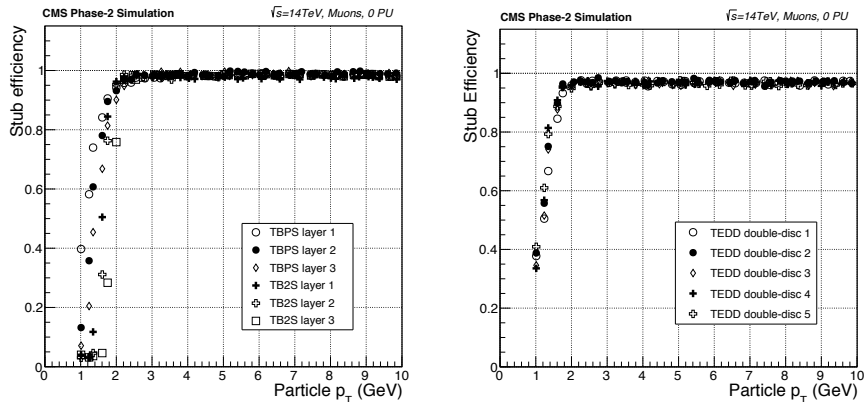


Figure 5

The stub finding efficiency as a function of particle  $p_T$  for muons, shown separately for the six barrel layers (left) and for the 5 disks (right). From Ref. (15).

TBPS layer 1, the turn-on curve for the stub finding efficiency is less sharp than in the outer layers due to the smaller bend of the track at smaller radii.

The full outer tracker design consists of 5,616 PS modules and 7,680 2S modules for a total of 13,296 modules. Each module is read out and controlled using one LpGBT module. The off-detector readout and control is handled by 216 DTC (Data, Trigger, and Control) boards. Each DTC is capable of controlling up to 72 front-end modules. The DTC receives data from the front-end modules and extracts the L1 accept data from the 40 MHz trigger data. The DTC unpacks the trigger data and assigns the stubs to the correct bunch crossing;

it also implements the data routing for the time and space multiplexing used by the track finder boards. The optical data links from the DTCs to the track finder boards operate at 25 Gbits/s.

## 2.2. Trigger Architecture

CMS utilizes a two-level trigger system to identify and select interesting collision events based on an initial L1 trigger, followed by a high-level trigger (HLT). The L1 trigger uses algorithms that run on custom electronics boards, while the HLT is implemented with algorithms that run on commercial CPUs. More recently, also algorithms running on GPUs are explored for the HLT. The L1 trigger has stringent constraints on the available processing time, referred to as the "latency", based on the available on-detector readout buffers that must temporarily store the information from different collision events until a signal is received as to whether or not to further process a given event. Strict constraints are also enforced on the total accepted event rate, following the design of the subsystem readout electronics. The CMS L1 trigger system for LHC Runs 1–3 has a latency of 4  $\mu\text{s}$  and a maximum readout rate of 100 kHz. For the HL-LHC operation, this will be increased to a latency of 12.5  $\mu\text{s}$  and a maximum output rate of 750 kHz. The increased latency is necessary to accommodate the processing of L1 tracking (33).

The entire CMS trigger system will be replaced for HL-LHC. At the core of the re-designed system is the added capability of L1 tracking. Figure 6 shows a schematic overview of the upgraded CMS L1 trigger architecture. Barrel and endcap calorimeter trigger systems will process high-granularity information from the calorimeters. Barrel, endcap, and overlap muon track finding systems will provide triggering of muons up to  $|\eta| < 2.5$ . The Global Track Trigger will reconstruct primary event vertices and define track-only based trigger objects. A two-stage *correlator* system will match L1 tracks with information from the calorimeter and muon systems, and perform a L1-adopted version of full event reconstruction (particle flow reconstruction) (34), to identify physics objects such as electrons, photons, muons, hadronic  $\tau$  leptons, jets, and energy sums. This list of objects will be propagated to the global trigger, which decides whether to retain the event for further processing (an L1 accept) or to discard it.

The inclusion of tracking is critical to maintain sufficiently low thresholds for electroweak physics and expanding the phase space of sensitivity for beyond-SM searches. Requiring e.g. multiples jets or leptons to originate from a common collision vertex (or  $z$  position) reduces significantly the event rates due to accidental matches of objects from different overlapping  $pp$  interactions. The definition of a complete L1 trigger menu is explored in Ref. (33), which with the inclusion of L1 tracking gives a total rate of approximately 500 kHz (keeping a 50% safety factor with respect to the maximum output rate of 750 kHz); without track information this would correspond to 4,000 kHz, a rate much too high to sustain. Incorporating tracking in the L1 trigger is thus essential in enabling the CMS HL-LHC physics program.

## 2.3. L1 Track Reconstruction Approaches

As described in Sect. 2.1, the CMS outer tracker for HL-LHC has been designed specifically to provide trigger primitives for L1 tracking. As part of validating the CMS tracker design, the implementation of the L1 tracking was investigated using different approaches, described in the Technical Design Report for the upgraded tracker (15). Three distinct approaches

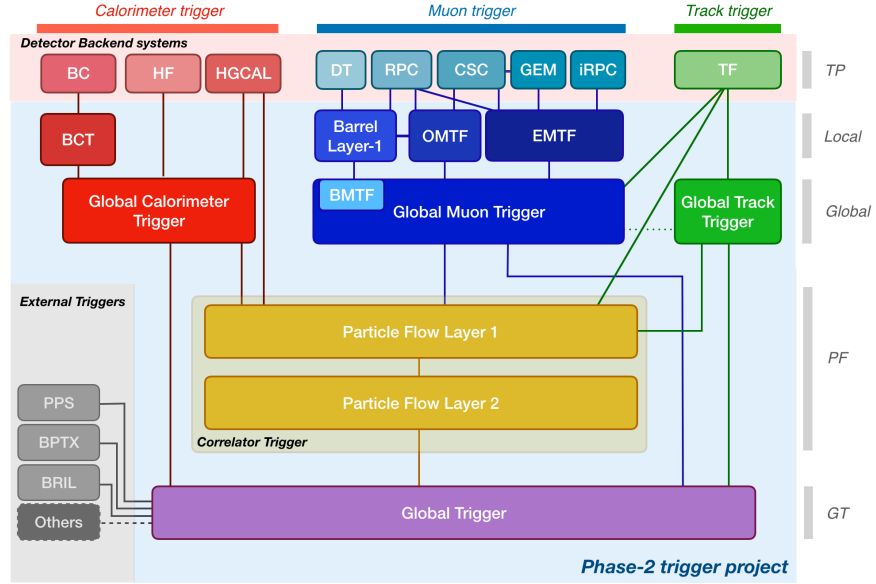


**Figure 6**

Overview of the CMS L1 trigger system for HL-LHC (14). The primary data flow is shown with solid lines; additional data paths are under study (dashes lines). The calorimeter trigger uses Trigger Primitives (TP) from the barrel calorimeter (BC), forward calorimeter (HF), and high-granularity calorimeter (HGCAL); it is composed of a Barrel Calorimeter Trigger (BCT) and a Global Calorimeter Trigger. The muon trigger receives inputs from the Drift Tubes (DT), Resistive Plate Chambers (RPC), Cathode Strip Chambers (CSC), and Gas Electron Multiplier chambers (GEM); it has a barrel layer-1 processor and muon track finders processing data from separate  $\eta$  regions (BMTF, OMTF, and EMTF, respectively). The Track Finders (TF) provide L1 tracks to a Global Track Trigger (GTT) as well as other components of the system. A two-stage Correlator Trigger performs correlations between tracks and other objects, including a Level-1 adopted version of particle-flow (PF) reconstruction. The Global Trigger (GT) receives all L1 objects and issues the final trigger decision.

were studied for performing the pattern recognition: the Tracklet approach, the Hough Transform approach, and the Associative Memory (AM) approach. The first two were fully based on FPGAs, while the latter used dedicated AM ASICs for pattern matching. Each pattern recognition approach was followed by a final track fit that improves track parameters and selects the best stub combinations in the case of combinatorics. The work required by the track fit varies depending on the pattern recognition approach; approaches that make use of coarse stub positions will have additional combinatorics and fake patterns that must be rejected during the final track fit. For all approaches the track fit was implemented in FPGAs.

The three pursued L1 tracking approaches have in common that they split the detector into smaller geometrical regions and utilize time multiplexing to distribute the tasks of performing the pattern recognition, track fitting, and duplicate removal to many different hardware components. Specifically, data are organized in regions in  $\eta-\phi$  (either in  $\phi$  sectors spanning the full  $\eta$  region, or in  $\eta-\phi$  trigger towers), and organized using a round-robin

time-multiplexing system with  $n$  identical copies of the system. The choice of detector segmentation and time-multiplexing factor depends on the algorithms and are described below. The described algorithms have been implemented in firmware, and validated using hardware demonstrators. For the demonstrators developed in support of Ref. (15), the stub data pre-processing in the DTCs was not fully specified; the different approaches therefore made different assumptions of its functionality.

This section discusses the common technology enablers necessary for L1 tracking, followed by a description of the different track finding approaches along with their implementations. The demonstrator systems and hardware platforms validating their feasibility are also described.

**2.3.1. Technology enablers.** The requirements for the HL-LHC track triggers in terms of data volume and processing needs are significantly higher than those of earlier track trigger implementations described in Sect. 1.3. However, over the last decade there has been rapid development in several technologies that enable the implementation of a hardware track trigger for the HL-LHC. The primary challenges are the input data rate, the processing requirements to find the tracks, and the latency required in the L1 trigger. The input data rate to the L1 track finding system is on the order of 30 Tbits/s, corresponding to about 15,000 stubs per bunch crossing every 25 ns. Sufficient computational processing power is required to implement the pattern recognition and track fitting algorithms. These algorithms have to process the roughly 15,000 stubs that arrive every 25 ns and find the tracks within about 4  $\mu$ s.

The rapid development in the last decade has provided optical links that operate at speeds of 25 Gbits/s. The use of these high speed links allows moving the data into the trigger system with a manageable number of links and with low latency. The rapid development of FPGAs provides the computational power required to implement the algorithms. The latest generation FPGAs have several thousands Digital Signal Processor (DSP) and block RAM units, and sufficient routing and logic support to implement the algorithms for the track finding (<https://www.xilinx.com/support/documentation/selection-guides/ultrascale-plus-fpga-product-selection-guide.pdf>, or <https://www.intel.com/content/dam/www/programmable/us/en/pdfs/literature/pt/intel-agilex-f-series-product-table.pdf>).

**2.3.2. Tracklet Approach.** The tracklet approach is an implementation of a traditional road search pattern recognition algorithm. Seeds are formed from stubs in adjacent layers or disks and matching stubs are found in the other detector layers. A final track fit is performed including the stubs matched to the seed. The tracklet approach makes use of the full stub position resolution when forming the seeds. This allows finding track candidates with high purity, which reduces the resources needed in the final track fit.

**2.3.2.1. Tracklet road search algorithm.** Tracklets, or the seeds, are formed from pairs of stubs in adjacent layers or disks. For each stub pair a trajectory is calculated, using the beam spot as a constraint in the transverse plane, and projections to other layers and disks computed. Using the projections to other layers and disks, matching stubs are found and used in the final track fit. These steps are illustrated in Fig. 7. The seeding is performed, in parallel, in multiple combinations of layers to ensure coverage and redundancy.

The main challenge in implementing this approach lies in organizing the data such that

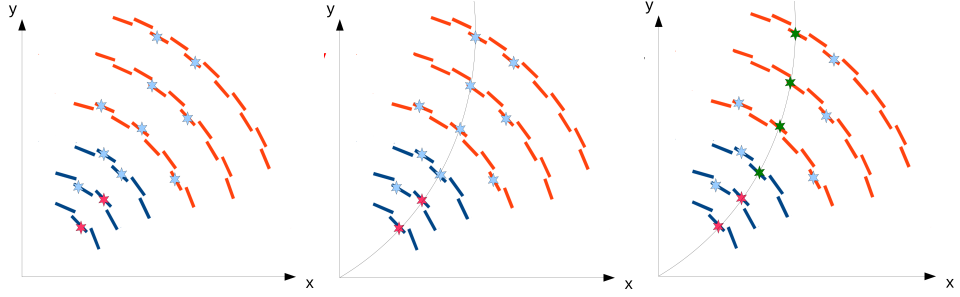


**Figure 7**

The tracklet approach forms seeds from pairs of stubs in adjacent layers or disks (left). The seed trajectories are projected to other layers/disks (middle) where stubs are matched and fit to form the final track (right). From Ref. (15).

sufficient processing capacity is available and truncation in the fixed latency environment is acceptable. This is achieved by dividing the data within each sector into finer regions, referred to as *virtual modules*. By forming stub pairs by combining stubs in pairs of virtual modules, the number of pairs that are not consistent with a real seed can be significantly reduced.

There are four main steps in the implementation of the tracklet approach; the stub organization, the tracklet formation, the stub matching, and the track fit. The first step organizes the stubs into regions based on the stub  $\phi$  position and the stub  $z$  or  $r$  position in the barrel and disks, respectively. This organization of the stubs allows for the tracklet finding to proceed by first forming candidate pairs of stubs. These stub pairs are required to be consistent with  $p_T > 2$  GeV and  $|z_0| < 15$  cm, and the bend of the two stubs must be consistent with the tracklet  $p_T$ .

Stub pairs that are selected are sent to the tracklet calculator where the precise track parameters as well as projections to other layers and disks are calculated. These projections are calculated with respect to a nominal layer or disk position, and the derivatives of the  $\phi$  and  $r$  ( $z$ ) positions are also evaluated. Stub matches in the other layers and disks are first looked for coarsely using the projection to the nominal radius; in a second stage the precise residuals are calculated using the exact stub position. The implementation selects the best stub match in each layer or disk based on the  $\phi$  residual.

**2.3.2.2. Linearized  $\chi^2$  track fit.** For the implementation of the final track fit in the tracklet approach, a linearized  $\chi^2$  fit is used that takes advantage of the information from the pattern recognition step. To match stubs to the projection from the seed, the residuals between the projections and stubs are calculated in both  $\phi$  and  $z$  (or  $r$  for disks). Using these residuals,  $\delta y_i$ , and linearizing the  $\chi^2$  fit, we can express the final track parameters  $u = (\rho^{-1}, \phi_0, t, z_0)$  where  $\rho$  is the signed radius of curvature related to  $q/p_T$ ,  $\phi_0$  is the track azimuthal angle at the IP,  $t = \sinh \eta$ , and  $z_0$  is the longitudinal impact parameter as

$$u = \bar{u} + \sum_i M_i \delta y_i \quad 4.$$

where  $\bar{u}$  are the track parameters from the seed and  $M$  is a weight matrix. The weight matrix can be precomputed, as to a good approximation it is independent of the parameters

except for stubs in the disks where it depends on the parameter  $t = \sinh \eta$  and the weights are tabulated for different ranges of  $t$ . The linear form of this equation means that the updated track parameters are obtained simply by multiply-and-add operations that are efficiently implemented in hardware.

Tracklet seeds with two or more matches in other layers or disks have a final track fit performed. These tracks have a minimum of four stubs. Since the track parameters from the tracklet seeds are accurately calculated based on the precise positions of the stubs, the final track fit provides a refinement to the track parameters. A linearized  $\chi^2$  fit that updates the track parameters of the seeds therefore works well.

**2.3.2.3. Tracklet demonstrator implementation.** The tracklet algorithm implementation relies on extensive parallelization, both in time and space. For the hardware demonstration of the algorithm the detector was divided into 28  $\phi$  sectors. Each time slice in a sector is processed by a *sector processor*, which is a dedicated hardware board with a modern FPGA with sufficient resources for the algorithm implementation. For the demonstrator implementation, a time-multiplexing factor of six was assumed, corresponding to each sector processor receiving a new event every 150 ns.

The algorithm is implemented in eight processing steps: 1) the VMRouter organizes the stubs into the virtual memories for the tracklet finding, 2) the TrackletEngine forms candidate stub pairs, 3) the TrackletCalculator calculates the precise trajectories and projections, 4) the ProjectionRouter organizes the projections into virtual modules, 5) the MatchEngine forms projection stub candidate matches, 6) the MatchCalculator calculates the precise residuals between the projections and stubs, 7) the FitTrack modules perform the final track fit, and 8) the PurgeDuplicate removes duplicate tracks. Two additional processing steps were used for matching stubs to projections pointing outside the sector where the tracklet was formed. The functionality of each of these modules were implemented in firmware (Verilog) and the complete project was built from connecting up many of these modules. The calculations, primarily done in the TrackletCalculator, MatchCalculator, and FitTrack modules, are implemented using the DSP blocks in the FPGAs. The other processing modules primarily organize the data by routing data to the relevant memories that act as buffers between the processing steps. The implementation is pipelined such that a different bunch crossing is processed at the same time in each of the eight processing steps.

The tracklet algorithm was implemented using the Calorimeter Trigger Processor (CTP7)  $\mu$ TCA board developed for the CMS Phase-1 upgrade (35). The CTP7 board has a Virtex-7 XC7VX690T FPGA and 63 input and 48 output optical links operating at speeds up to 10 Gbits/s. The demonstrator system implemented one time slice for one central sector and its two neighboring sectors. A separate board was used as the source of input stubs to the track finder boards and as the receiver of the final tracks (36).

**2.3.3. Hough Transform + Kalman Filter Approach.** The Hough transform is a common tool for pattern recognition (37) and is implemented in the track finding to identify curved trajectories in the  $r - \phi$  plane. In the approach studied for Ref. (15), the hit patterns from the Hough transform are processed by a Kalman filter as the final track fit (38).

**2.3.3.1. Hough transform pattern recognition.** The trajectory of a charged particle produced at the origin (interaction point) that travels through a uniform magnetic field,  $B$ ,

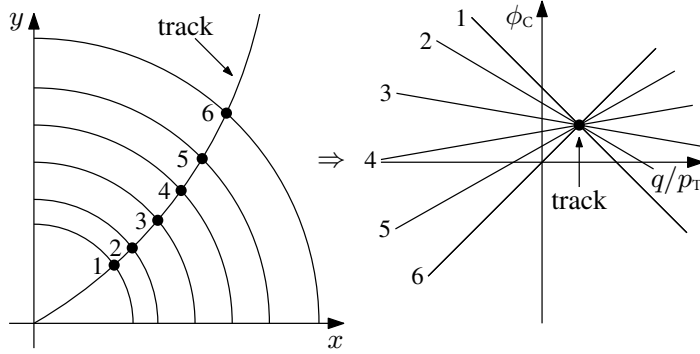


**Figure 8**

Illustration of the Hough Transform idea for finding particle trajectories. The left-hand side shows a particle trajectory with six stubs in different layers. The right-hand side shows the lines of possible  $\phi_c$  and  $q/p_T$  for each of the six stubs. The point where these six lines cross corresponds to the track parameters for the trajectory. Adopted from Ref. (38)

satisfies

$$\phi_0 = \phi - \frac{qB}{2p_T} \cdot r \quad 5.$$

where  $r$  and  $\phi$  are the trajectory coordinates,  $\phi_0$  is the angle of the trajectory at the production point,  $q$  is the particle's electric charge, and  $p_T$  the transverse momentum.

To reduce the correlation between the  $r$  and  $\phi$  positions it is convenient to use  $r_c = r - C$ , where  $C$  is a radius approximately in the middle of the detector. This gives

$$\phi_c = \phi - \frac{qB}{2p_T} \cdot r_c \quad 6.$$

where  $r_c$  is a signed radial position and  $\phi_c$  is the trajectory angle at the radius  $C$ . For each stub, at a given  $r_c$  and  $\phi$ , Eq. 6 describes a straight line in the  $\phi_c$  vs.  $q/p_T$  plane. For a track with six stubs, as shown in Fig. 8, each of these stubs will form a unique line, where the slope is a function of the radial position of the stub. If the stubs belong to the same particle trajectory these lines will all go through the same  $(q/p_T, \phi_c)$  point. Tracks can therefore be identified by looking for points in the  $(q/p_T, \phi_c)$  plane where multiple lines overlap. In an FPGA this is implemented using an array to find bins with multiple entries. This gives the track candidates with an estimate of the track parameters in the  $r - \phi$  plane.

**2.3.3.2. Kalman filter track fit.** The Hough transform pattern recognition produces track candidates that can have multiple stubs in a given layer and the final fit must therefore filter the stubs used to form the track. This filtering and fitting is implemented using a Kalman filter (39). The Kalman filter begins with an initial seed estimate of the track parameters and their uncertainties, referred to as a *Kalman state*. Here, the seed is provided from the Hough transform. The Kalman state is updated, iteratively, starting from stubs in the innermost layers. The seed trajectory is projected to the next layer or disk and the state is duplicated if there are more than one stub. The track parameters are updated using the position information from the next stub. The fit allows for one missing layer.



This process is repeated until four stubs has been added to the trajectory. The pattern recognition (Hough transform) requires at least five stubs, while a successful fit requires four stubs.

**2.3.3.3. Hough transform + Kalman filter demonstrator implementation.** The Hough transform + Kalman filter approach is implemented as a Track Finding Processor with four distinct components: (i) Geometric Processor (GP), responsible for the pre-processing of stub data; (ii) Hough Transform (HT), coarsely grouping stubs consistent with high- $p_T$  trajectories; (iii) Kalman Filter (KF), second stage track cleaning and track fitting; (iv) Duplicate Removal (DR), removing duplicate tracks. This approach has been implemented in firmware on FPGAs. The track finding processor handles 1/8 of the detector, an octant, and uses a time-multiplexing factor of 36.

The first step involving the Geometric Processor carries out an initial processing of the stub data as it is assumed to be received from the DTCs into an extended 64-bit format, with motivation to minimize the downstream logic requirements in the Hough Transform. It also assigns stubs to 36 sub-sectors ( $2\phi \times 18\eta$ ).

Each Track Finder Processor uses 36 HT arrays running in parallel, each processing stub data consistent with the corresponding geometric region defined by the Geometric Processor; one GP sub-sector corresponds to one HT array. The HT array is split into two pipelined stages, first the filling of the array with stubs, and second the readout of the found track candidates. Each of these two stages processed one stub at 240 MHz. The HT array is implemented in firmware as 32 *columns* in  $|q/p_T|$  and 64 *rows* in  $\phi$ .

The Kalman filter was implemented in two parts, a data-flow component, which carries out the matrix operations described by the Kalman formalism (state updater and the calculation of track parameters and covariance matrix), as well as a control-flow component, which manages the stub and state data.

The Hough transform + Kalman filter approach was implemented using the Master Processor 7 (MP7)  $\mu$ TCA boards developed for the CMS Phase-1 trigger upgrade (40). The MP7 board uses the same Virtex-7 FPGA as the CTP7 board. The demonstrator system used five MP7 boards to implement the track reconstruction for one time slice for one detector octant. One MP7 board was used as the Geometrical Processor, two boards were used for the HT pattern recognition, and two boards for the KF track fitter. In addition, two MP7 boards were used as data sources and one was used as a sink for the produced tracks (38).

**2.3.4. Associative Memory + FPGA Approach.** The associative memory approach uses a content addressable memory (CAM) ASIC to implement the pattern recognition. The AMs allow simultaneous matching to a large number of patterns, providing a fast response once all hits have been loaded. The patterns are coarse hit positions, super strips, on the modules. The AM returns all roads, i.e. patterns matched that have a minimum number of matched stubs. The final  $\chi^2$  track fit implements filtering to reject wrong stub combinations.

**2.3.4.1. Associative memory pattern recognition.** In the AM approach the detector is divided into trigger towers. The demonstration system explored for Ref. (15) had 48 regions (8 in  $\phi$  and 6 in  $\eta$ ), and a time-multiplexing factor of 20. Based on the demonstration studies, about 1M patterns were determined to be required for each trigger tower and time-multiplexing slice. The design assumed that individual AM chips could be produced with

about 150k patterns. The stub data received from the front-end is routed by the Data Organizers (DO) to the appropriate processing unit that is handling the stub for that BX. The stubs are converted to super strips and transmitted to the AM. The super strips vary in width from about 1 mm at the inner radii up to about 10 mm at outer radii. The larger strip size at outer radii optimizes the number of patterns required; larger strips at outer radii compensates for multiple scattering and lower occupancy. Once all stubs are loaded into the AM the pattern recognition is performed. Stubs that are on roads found by the AM are passed to the Combination Builder that forms the different stub combinations from stubs within each road. These are then passed onward to the track fitter stage.

**2.3.4.2. Track fitting for the AM approach.** For the AM approach, a somewhat different implementation of a linearized  $\chi^2$ -fit is used, which is based on a principal component analysis (PCA) technique (41). This fit obtains the track parameters by multiplying a vector of stub coordinates by an appropriate translation matrix. Again, the matrix multiplication can be efficiently implemented with low latency using the DSP resources in modern FPGAs. Tabulating the transformation matrix is very simple for a set of hits in a cylindrical geometry, while in a geometry with disks or varying radial positions within a layer, the matrix depends on the track parameters, particularly  $\eta$ . The fit used has implemented a method to project the hit positions to fixed radial positions.

**2.3.4.3. Associative memory + FPGA demonstrator implementation.** The AM+FPGA approach was implemented using AM chips that perform the stub selection and pattern recognition using coarse stub position information, followed by track fitting implemented in an FPGA using stubs at full resolution. For each of the 48 trigger towers, the AM chips are preloaded with hit patterns representing possible valid trajectories for that tower's geometry. In the first processing step, stubs are received and routed to the pattern recognition mezzanine board for the relevant trigger tower and time-multiplexing slice. The data organizer formats and loads the data into the AM. When all data has been loaded the AM pattern recognition is performed and the matched patterns are read out. The DO retrieves the stubs on the matched patterns and forward them to the track fit.

The demonstration of the AM+FPGA approach is based on the Pulsar2b ATCA board (42). The Pulsar2b board uses the Xilinx Virtex-7 690T FPGA and allows board-to-board communication across the ATCA backplane. The backplane communication is used in the demonstrator to implement the time multiplexing. In the demonstrator the Pulsar2b served both as the data source and the Pattern Recognition Board (PRB). The Pulsar2b supports two Pattern Recognition Mezzanine (PRM) boards that implements the pattern recognition using AMs. For the demonstrator two types of PRMs are used. One is based on the AM06 ASIC (43) and provided the pattern density required. However, as this AM ASIC was not developed for a L1 application it did not meet the latency or data throughput requirements. The second PRM was developed for AM ASICs that were under development at the time of the demonstrator. The PRM was developed such that it could support an FPGA instead of the AM ASIC. For the demonstrator, the PRM with the FPGA option is used; the FPGA provide a clock cycle accurate proxy for the AM ASIC. This allowed the demonstration to meet the latency requirement but did not have the pattern density that is ultimately required, but allowed demonstration of the rest of the system.

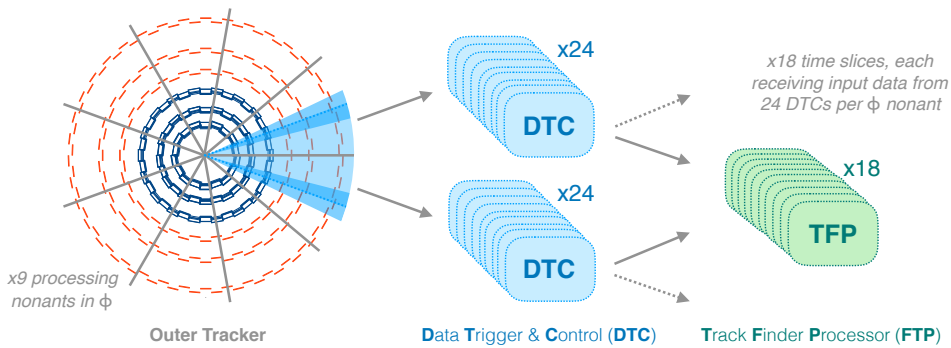


**Figure 9**

Schematic overview of the data flow from the outer tracker, divided into nine "nonants" in  $\phi$ , each read out by 24 DTC boards. From the DTCs, the stub data is forwarded to the track finder processor boards.

## 2.4. HL-LHC Track-Finding System

CMS has designed a novel tracker based on the concept of  $p_T$  modules that will provide stub primitives at 40 MHz for the L1 tracking. The ability to reconstruct tracks in hardware at the L1 trigger level was demonstrated using three different approaches. Following these demonstrations, CMS has adopted a hybrid approach that makes use of the tracklet approach for the pattern recognition and the Kalman filter for the final track fit. This choice allows the implementation of the full algorithm in commercial FPGAs without the need to develop custom ASICs for the pattern recognition.

**2.4.1. Hybrid implementation.** The three described approaches for pattern recognition and track fitting were pursued to demonstrate the feasibility of L1 tracking at 40 MHz in the HL-LHC environment with an average of 200 pileup interactions. The conclusion of the studies was that all three methods were feasible and could implement L1 tracking with comparable performance and meeting the latency requirement of about  $4 \mu\text{s}$ . For the ultimate HL-LHC system, CMS has decided to pursue an all-FPGA based approach. The primary reason for this choice is (15) to reduce the risks associated with the development of the AM ASIC, which involves new technologies such as 28 nm or 3D integration.

Following the choice of an all-FPGA solution, CMS is pursuing a hybrid implementation. The tracklet algorithm is used for finding the candidate tracks, i.e. seeds are found and matched to stubs in other layers and disks, while the final track fit is performed using the Kalman filter. The combination of the tracklet approach with precise seeds and the iterative Kalman filter provides optimal performance. A schematic overview of the data flow from the outer tracker through the DTC boards and onward through the track finder processing is shown in Fig. 9. The hybrid system assumes a time-multiplexing factor of 18 and a division in  $\phi$  into nine "nonants".

**2.4.2. Hardware platforms.** Developments of hardware prototypes and plans for the ultimate system are underway to define the track finder boards that will be used for the HL-LHC system. The Apollo (44) platform will be used for the track finder processing

boards, while the Serenity (45) platform will be used for the DTC boards. Both platforms are based on the ATCA standard, and contain separate components for providing the necessary services and performing the data processing. The Apollo has a *Service Module* (SM) that provides infrastructure components, including the required ATCA Intelligent Platform Management Controller (IPMC) (46), powering, clock, and a system-on-module computer. A *Command Module* (CM) can be customized for the particular application, here the track finder processing, and contains two large FPGAs, several hundred optical fiber interfaces supporting link speeds of up to 28 Gbits/s, and memories. Similarly, the Serenity platform consists of a carrier card that provides the required services, such as powering, clocking, optical interfaces, interconnections between FPGAs, IPMC functionality, and an on-board CPU for controlling the board. Daughter cards host FPGAs that are responsible for the data processing, in this case, the DTC functionality.

**2.4.3. Displaced tracking.** The CMS L1 track finding approaches discussed so far are developed for reconstructing prompt particles. However, the unique design of the CMS Outer Tracker for HL-LHC also has the potential of reconstructing long-lived charged particles that may have escaped detection thus far. Long-lived charged particles that decay a macroscopic distance away from the primary interaction point but prior to traversing the outer tracker would appear as *displaced* trajectories. With the vast physics motivation to search for such particles, see e.g. Ref. (47) for a comprehensive review, efforts are underway to explore the full potential and technical feasibility of extending the CMS L1 tracking to reconstruct displaced trajectories. Proposed initially in Ref. (48) and further explored in Ref. (49), the CMS L1 tracking could identify trajectories with displacements in the plane transverse to the beam line as large as about 10 cm. In particular, the physics case of a Higgs boson decaying to two new light scalars that in turn decay to jets, where the scalars have a sufficiently large lifetime so that the jets appear displaced from the primary vertex, is studied (50, 51). This process is nearly free from Standard Model background contributions, and with the current CMS detector would fail to be selected in the L1 trigger, while when incorporating displaced tracking, such rare exotic decays could be probed using the large HL-LHC data set. The dedicated reconstruction of displaced trajectories could be incorporated in the tracklet pattern recognition algorithm through the addition of *triplet* seeds that remove the constraint to the beamspot and instead adds a third stub (48, 52).

**2.4.4. Expected performance.** The expected performance of the L1 track reconstruction has been studied using simulated data and validated with hardware demonstration systems. The performance metrics used include the identification efficiency of different types of charged particles, such as isolated muons or electrons, and charged particles from the decays of top quark–anti-quark pairs ( $t\bar{t}$ ), which include charged particles produced in the dense environment of jets. Other performance metrics are the expected track parameter resolutions ( $p_T$ ,  $\phi_0$ ,  $\eta$ ,  $z_0$ ), and the total rate of tracks per event.

Examples of the expected L1 tracking performance are illustrated in Fig. 10. It shows the expected L1 track reconstruction efficiency (top left) as a function of pseudorapidity for tracks in  $t\bar{t}$  events overlaid with an average of 200 pileup interactions, using the hybrid algorithm (52), as well as the expected  $z_0$  resolution, corresponding to intervals that encompass either 68% or 90% of all tracks with  $p_T > 2$  GeV (top right). At central  $\eta$ , the resolution is about 1 mm, while it is less precise at higher  $\eta$  as a consequence of the CMS outer tracker geometry with tilted PS modules. Also shown (bottom left) is the expected

track rate per  $\phi$  sector (one ninth of the detector) for a minimum  $p_T$  threshold of 2 GeV. Finally, the possible extension to reconstructed displaced trajectories that do not originate from the origin, consistent with possible long-lived particles, is shown (bottom right) as the efficiency as a function of the transverse impact parameter ( $d_0$ ) for displaced muons in events without pileup. This extended, displaced tracking has the potential to significantly extend the  $d_0$  coverage.

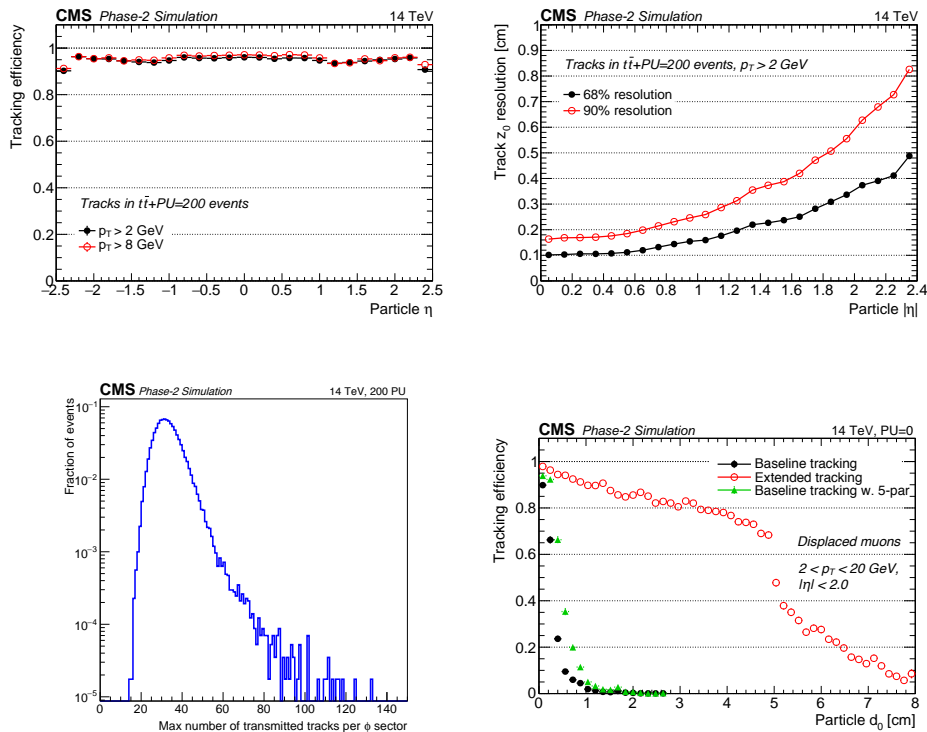


**Figure 10** L1 track finding efficiency as a function of particle  $\eta$  (top left) and track longitudinal impact parameter resolution as a function of  $|\eta|$  (top right) for charged particles from top quark pair events with an average of 200 additional pileup interactions; L1 track rate per  $\phi$  sector for a minimum  $p_T$  threshold of 2 GeV (bottom right); L1 track finding efficiency as a function of transverse impact parameter for tracks corresponding to long-lived particles (bottom left), showing the possible enhancement in efficiency from the extended, displaced tracking (14).

### 3. ATLAS HARDWARE-BASED TRACKING FOR HL-LHC

The ATLAS experiment has designed a new tracker for the HL-LHC upgrade (53, 54). Similar to CMS, the original ATLAS tracker must be replaced as it cannot handle the much higher data rates and radiation exposure at the HL-LHC. The layout of the ATLAS tracker for the HL-LHC is shown in Fig. 11. It is based on an all-silicon design with pixel sensors in the inner regions where the occupancies are highest and strip sensors in the outer regions. The acceptance of the strip detectors covers the range  $|\eta| < 2.7$  while the pixels extend

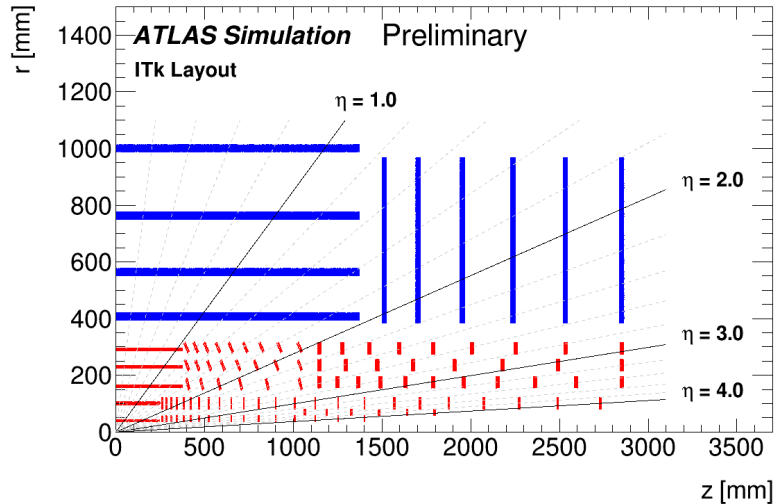


**Figure 11**

The proposed geometry for the ATLAS inner tracker upgrade for the HL-LHC is an all Si based design. The innermost region,  $r < 350$  mm, is instrumented with pixel detectors in a configuration with five barrel layers and four rings in the forward region. The radial region  $350 < r < 1000$  mm is instrumented with strip detectors with four barrel layers and six forward disks. From Ref. (54).

coverage to  $|\eta| < 4.0$ . Stereo angles are implemented in the strip detectors to provide a second coordinate measurement.

The ATLAS experiment’s use of tracking in the trigger system differs from that of CMS described earlier in that the ATLAS tracker does not provide trigger primitives. Hence ATLAS has chosen a different approach to hardware-based tracking where full-detector trajectory reconstruction is not performed in the first stage of the trigger system. The ultimate trigger system design is under development; here we present the assumptions outlined in Ref. (55).

An overview of the ATLAS trigger system is shown in Fig. 12, where both the baseline architecture with a single-level hardware trigger and the evolved architecture with a two-level hardware trigger, also referred to as an “L0/L1” architecture, are shown. The baseline architecture operates a single Level-0 (L0) hardware trigger using information from the calorimeter and muon detector systems, with a maximum readout rate of 1 MHz and latency of  $10 \mu\text{s}$ . ATLAS is additionally maintaining upgrade projects with flexibility of possibly including L1 track reconstruction through the L0/L1 architecture, where regional tracking is operating at an input rate of 4 MHz. The evolved architecture is in particular intended to mitigate risks associated with uncertainties in hadronic trigger rates and occupancies in the inner pixel detector layers (55).

The primary goal of incorporating tracking in the ATLAS trigger is to reconstruct tracks in hardware as an input to the HLT to reduce CPU usage. It is foreseen to use pattern recognition with AMs (see Sect. 2.3.4.1), in combination with track fitting in FPGAs, though different options are under consideration. In the baseline architecture, the so-called Hardware Tracking for the Trigger (HTT) is expected to perform a combination of regional

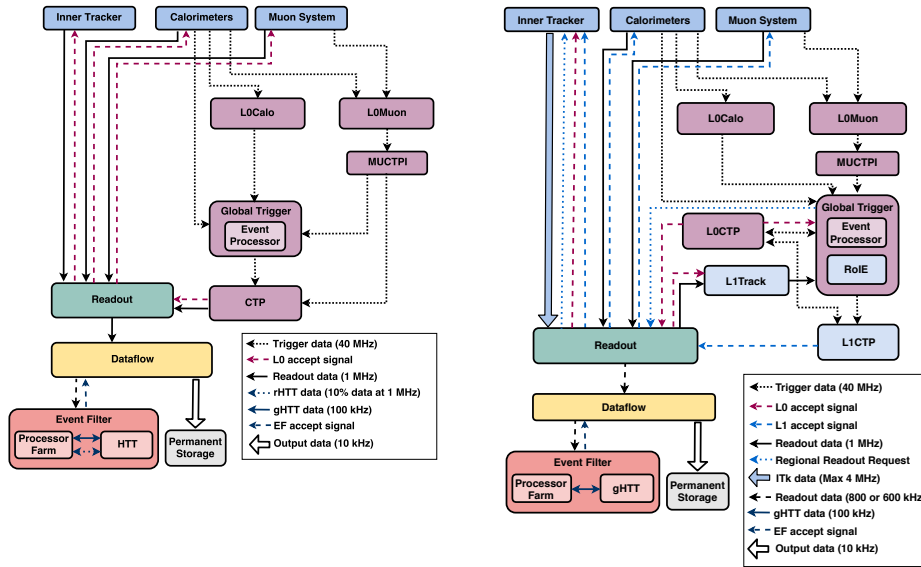


Figure 12

Diagram of the ATLAS baseline TDAQ system (left) with a single-level hardware trigger and the evolved TDAQ system (right) with a two-level hardware trigger. From Ref. (55).

(seeded) and global (full-detector) tracking. Regional tracking (rHTT) would be performed for approximately 10% of the detector with an input event rate of 1 MHz, seeded by the L0 trigger that utilizes information from the calorimeter and muon systems only, while the global full-detector tracking (gHTT) would be performed as a second step, with an input rate of 100 kHz. The HTT system is largely based on the developments toward the FTK system that was intended to be used by ATLAS in LHC Run-3 (22). The rHTT is expected to reconstruct trajectories with  $p_T > 2$  GeV, whereas the gHTT would target  $p_T > 1$  GeV, both covering the acceptance region of  $|\eta| < 4.0$ . Since the HTT is not operating in the first-level trigger, the latency constraints are less stringent than for the CMS L1 track trigger system, and the allowed latency is of the order of 100  $\mu$ s.

The HTT system is foreseen to be based on 48 independent HTT units, providing track reconstruction for a dedicated  $\eta - \phi$  region, each corresponding to one ATCA shelf. The track finding is divided in two steps, implemented in common Tracking Processor (TP) boards. The first stage performs the pattern recognition through AM ASICs hosted in TP boards with Pattern Recognition Mezzanines, and in the second stage, the track fitting is carried out in FPGAs in TP boards with Track Fitting Mezzanines.

An alternative FPGA-based, Hough Transform implementation of the pattern recognition is being studied as an alternative to the use of the Associative Memory ASIC. Both the baseline AM-based as well as the FPGA-based implementations provide flexibility to enhance the selection of long-lived particles (56).

## 4. SUMMARY

One of the main challenges to fully explore the HL-LHC potential involves maintaining sufficiently low thresholds to efficiently trigger on the important electroweak physics processes in the high pileup environment. Including information from the charged-particle tracking detectors in the hardware trigger will provide a major new handle to control the trigger rates while maintaining thresholds to efficiently trigger on  $H/W/Z$  boson production. The inclusion of tracking improves the quality of almost all trigger objects, including muon, electrons, hadronic  $\tau$ s, jets, missing transverse energy, and energy sums.

The CMS Collaboration has designed a new tracker for the HL-LHC upgrades where providing trigger primitives is a key novel capability. The upgraded outer tracker will be constructed using a new type of modules,  $p_T$  modules, which consist of two Si sensors spaced a few millimeters apart. By correlating hits in the two sensors in logic implemented on the module, trigger primitives (stubs) can be formed. These stubs, required to be consistent with charged particles with a transverse momentum above 2 GeV, can be read out at the full bunch crossing rate of 40 MHz. They serve as the input to a backend L1 track finding system.

CMS has demonstrated the ability to efficiently reconstruct L1 tracks in dedicated hardware within the latency requirements of the L1 trigger. Three different approaches were pursued for the pattern recognition plus track fitting: the tracklet road search algorithm, the Hough transform plus Kalman Filter, and the Associative Memory approach. All three approaches make use of time multiplexing, where data from different bunch crossings are distributed to different processing units, and a spatial division of the detector. Each of these approaches were shown to have the potential to work and CMS is pursuing an all-FPGA based approach that uses the tracklet road search algorithm for the pattern recognition, combined with the Kalman filter for the final fit.

Prototypes for the hardware for the L1 tracking, the Serenity and Apollo boards, have been developed. The Serenity board will implement the DTC functionality, which will unpack and organize the data into the correct processing boards and time multiplexing slices. The Apollo board will implement the track finding algorithm.

The ATLAS Collaboration is pursuing a tracker design optimized for offline reconstruction for their HL-LHC upgrades. In the baseline trigger architecture, hardware-based track reconstruction is used as an input to the software-based high-level trigger. The implementation is planned to use associative memories for pattern finding and FPGA-based linearized track fitting. An alternative architecture is envisaged, where low-latency regional track reconstruction is included as part of the L1 hardware trigger with an input rate of 4 MHz.

Hardware-based, low latency track reconstruction will provide an important handle for the triggers at HL-LHC. The use of track information will provide an essential tool to mitigate the effects of high pileup. Significant work has been performed to demonstrate the feasibility of these approaches for the planned detector designs, as documented in the experiments' technical design reports for the HL-LHC upgrades. These upgrade projects are now proceeding to the implementation stage. The hardware will be installed in the experiments during LHC upgrades in 2025-2027 and operations with the upgraded detectors are scheduled to start in late 2027.



## DISCLOSURE STATEMENT

The authors were early proponents of the development of the CMS track trigger and the tracklet approach in particular.

## ACKNOWLEDGMENTS

The authors thank their CMS collaborators and ATLAS friends for useful discussions and insights. A.R. is grateful to the U.S. National Science Foundation for its continued support under grant NSF-PHY-1912813.

## LITERATURE CITED

1. Brüning O, et al. LHC Design Report. Tech. Rep. CERN-2004-003, CERN, Geneva (2004)
2. Evans L, Bryant P. *J. Instrum.* 3:S08001 (2008)
3. ATLAS Collaboration. *J. Instrum.* 3:S08003 (2008)
4. CMS Collaboration. *J. Instrum.* 3:S08004 (2008)
5. Zimmermann F. *PoS EPS-HEP 2009:140* (2009)
6. Apollinari G, et al. High-Luminosity Large Hadron Collider (HL-LHC): Technical Design Report V. 0.1. Tech. Rep. CYRM-2017-004, CERN (2017)
7. ATLAS Collaboration. Letter of Intent for the Phase-II Upgrade of the ATLAS Experiment. Tech. Rep. CERN-LHCC-2012-022. LHCC-I-023, CERN (2012)
8. ATLAS Collaboration. ATLAS Phase-II Upgrade Scoping Document. Tech. Rep. CERN-LHCC-2015-020. LHCC-G-166, CERN (2015)
9. CMS Collaboration. Technical Proposal for the Phase-2 Upgrade of the CMS Detector. Tech. Rep. CERN-LHCC-2015-010, CERN (2015)
10. CMS Collaboration. CMS Phase II Upgrade Scope Document. Tech. Rep. CERN-LHCC-2015-019. LHCC-G-165, CERN (2015)
11. ATLAS and CMS Collaborations. Report on the Physics at the HL-LHC and Perspectives for the HE-LHC. Tech. Rep. CYRM-2019-007, CERN (2019)
12. ATLAS Collaboration. *Eur. Phys. J. C*:77: 317 (2017)
13. CMS Collaboration. *J. Instrum.* 12:P01020 (2017)
14. CMS Collaboration. The Phase-2 Upgrade of the CMS Level-1 Trigger. Tech. Rep. CERN-LHCC-2020-004, CERN (2020)
15. CMS Collaboration. The Phase-2 Upgrade of the CMS Tracker. Tech. Rep. CERN-LHCC-2017-009, CERN (2017)
16. LHCb Collaboration. LHCb Trigger and Online Upgrade Technical Design Report. Tech. Rep. CERN-LHCC-2014-016, LHCb-TDR-016, CERN (2014)
17. Bailey S, et al. *Nucl. Instrum. Meth.* A518:544 (2004)
18. Iwasaki Y, et al. *IEEE Trans. Nucl. Sci.* 58:1807 (2011)
19. Gerndt EKE, Xella S. *Nucl. Instrum. Meth.* A446:264 (2000)
20. Adelman J, et al. *Nucl. Instr. Meth. A* 572:361 (2007)
21. Olsen J, et al. *IEEE Trans. Nucl. Sci.* 51:345 (2004)
22. Shochet M, et al. Fast TracKer (FTK) Technical Design Report. Tech. Rep. CERN-LHCC-2013-007. ATLAS-TDR-021, CERN (2013)
23. Thomson EJ, et al. *IEEE Trans. Nucl. Sci.* 49:1063 (2002)
24. Holm S, et al. *IEEE Trans. Nucl. Sci.* 47:895 (2000)
25. Dell'Orso M, Ristori L. *Nucl. Instrum. Meth.* A287:436 (1990)
26. Abolins M, et al. *IEEE Trans. Nucl. Sci.* 51:340 (2004)
27. Adams T, et al. arXiv:physics/0701195 [physics.ins-det] (2007)
28. Sottocornola S. *Frascati Phys. Ser.* 67:41 (2018)

29. Ceresa D, et al. *PoS TWEPP*2018:166 (2019)
30. Prydderch ML, et al. *PoS TWEPP*-17:001 (2018)
31. Nodari B, et al. *PoS TWEPP*2018:099 (2019)
32. Mendez JM, Baron S, Kulis S, Fonseca J. *PoS TWEPP*2018:059 (2019)
33. CMS Collaboration. The Phase-2 Upgrade of the CMS L1 Trigger Interim Technical Design Report. Tech. Rep. CERN-LHCC-2017-013, CERN (2017)
34. CMS Collaboration. *J. Instrum.* 12:P10003 (2017)
35. Svetek A, et al. *J. Instrum.* 11:C02011 (2016)
36. Bartz E, et al. *J. Instrum.* 15:P06024 (2020)
37. Hough PVC. Method and means for recognizing complex patterns. Tech. Rep. U.S. patent 3,069,654 (1962)
38. Aggleton R, et al. *J. Instrum.* 12:P12019 (2017)
39. Billoir P, Qian S. *Nucl. Instrum. Meth.* A294:219 (1990)
40. Compton K, et al. *J. Instrum.* 7:C12024 (2012)
41. Clement E, et al. *Nucl. Instrum. Meth.* A935:95 (2019)
42. Ahuja, S. and others. A Full Mesh ATCA-based General Purpose Data Processing Board (Pulsar II). Tech. Rep. FERMLAB-TM-2650-E, Fermilab (2017)
43. Annovi A, et al. *J. Instrum.* 12:C04013 (2017)
44. Hazen ES, et al. *PoS TWEPP*2019:120 (2020)
45. Rose A, et al. *PoS TWEPP*2018:115 (2019)
46. Mendez J, et al. *J. Instrum.* 12:C03010 (2017)
47. Curtin D, et al. *Rep. Progress Phys.* 82:116201 (2019)
48. Gershtein Y. *Phys. Rev. D* 96:035027 (2017)
49. Gershtein Y, Knapen S. *Phys. Rev. D* 101:032003 (2020)
50. Cepeda M, et al. arXiv:1902.00134 [hep-ph] (2019)
51. Alimena J, et al. arXiv:1903.04497 [hep-ex] (2019)
52. James T arXiv:1910.12668 [physics.ins-det] (2019)
53. ATLAS Collaboration. Technical Design Report for the ATLAS Inner Tracker Strip Detector. Tech. Rep. CERN-LHCC-2017-005, ATLAS-TDR-025, CERN (2017)
54. ATLAS Collaboration. Expected Tracking Performance of the ATLAS Inner Tracker and the HL-LHC. Tech. Rep. ATL-PHYS-PUB-2019-014, CERN (2019)
55. ATLAS Collaboration. Technical Design Report for the Phase-II Upgrade of the ATLAS TDAQ System. Tech. Rep. CERN-LHCC-2017-020. ATLAS-TDR-029, CERN (2017)
56. Mårtensson M, et al. *J. Instrum.* 14:P11009 (2019)